Available online at www.sciencedirect.com
ScienceDirect
Advances in Space Research 38 (2006) 461–465
ADVANCES IN SPACE RESEARCH (a COSPAR publication)
www.elsevier.com/locate/asr

Properties of structured coronal mass ejections in solar cycle 23

H. Cremades *, V. Bothmer, D. Tripathi

Max-Planck-Institut für Sonnensystemforschung, D-37191 Katlenburg-Lindau, Germany

Received 3 November 2004; received in revised form 25 January 2005; accepted 26 January 2005

Abstract

The Solar and Heliospheric Observatory has provided to date doubtlessly the best dataset of coronal observations ever taken over the course of a solar cycle. Structured coronal mass ejections, i.e. events with clear white-light fine structures, have been selected from the dataset of the large angle spectroscopic coronagraph during the period 1996–2002. Their source regions in the low corona and photosphere have been deduced by analyzing data from the Extreme-ultraviolet Imaging Telescope and Michelson Doppler Imager onboard the Solar and Heliospheric Observatory and from ground-based Hα measurements. Based on this subset of coronal mass ejections, originally compiled to study their three-dimensional configuration, we have analyzed the variation of their properties during the present solar cycle. These properties include latitude and tilt angle of source regions of coronal mass ejections, position angle of coronal mass ejections, and deviation of coronal mass ejections with respect to their corresponding source regions. The results show a pronounced and systematic confinement of position angles at equatorial latitudes and equatorward deviations during low solar activity. In contrast, fluctuating position angles and deviations in all directions were found at times of high solar activity. A method to explain the observed deflections is presented.

Keywords: Sun, corona; Sun, coronal mass ejections (CMEs); Sun, prominences

1. Introduction

Coronal mass ejections (CMEs) are the direct outcome of the Sun's dynamic nature. Their importance regarding solar physics processes and space weather effects is well established. They have been the subject of numerous studies since their discovery in the early 1970s by space borne coronagraphs (Gosling et al., 1974; Tousey et al., 1974). Soon after, they were found to be associated with flares and prominence eruptions (e.g., Munro et al., 1979). It was not until 1984 that they were defined and termed as coronal mass ejections by Hundhausen et al. (1984).

In a previous study of Cremades and Bothmer (2004), henceforth called C&B, a set of 276 "structured" CMEs had been selected from the full set of Large Angle Spectroscopic Coronagraph (LASCO) C2 images during the period 1996–2002, in order to understand better the three-dimensional configuration of CMEs. The frequency distribution in time of this set of CMEs followed the sunspot cycle, in close correspondence with the distribution of the total number of CMEs (see Fig. 3 in C&B). The photospheric and low coronal source regions could be uniquely identified for 124 of the events, using observations from the EUV Imaging Telescope (EIT) and the Michelson Doppler Imager (MDI) onboard the Solar and Heliospheric Observatory (SOHO), and Hα images from ground-based observatories at Meudon and Big Bear. The source regions were identified on the basis of pre- and post-eruptive features, such as eruptive prominences, flares, dimmings, post eruptive loops, and outward motions of coronal material. Additionally, spatial and temporal correlation between the CME and its candidate source region was required.

* Corresponding author. Tel.: +49 5556 979 464.
E-mail address: cremades@mps.mpg.de (H. Cremades).

0273-1177/$30
doi:10.1016/j.asr.2005.01.095

Here, we concentrate in the variation of various structured CME parameters during the rising and maximum phases of solar cycle 23. These have been subdivided into two main categories: (1) parameters related to the source region characteristics, and (2) paramenters directly associated with the CMEs themselves and their spatial behavior with respect to their associated source regions.

2. CME source region characteristics

2.1. Neutral line tilt evolution in time

The structured CMEs' source regions were uniquely related to the regions of opposite polarities, when traced back to MDI magnetograms (see C&B). The source regions' neutral lines have been approximated by straight lines, though they might present substantial curvature in individual cases. Neutral lines may also be very long, with only a portion of the length involved in the eruption. The source region extension has been defined based solely on the portion of the neutral line over which a disappearing filament was lying or above which post-eruptive arcades formed, as in C&B. This lineal approach to determining the structured CMEs' source regions yielded the temporal variation of their tilts, represented in Fig. 1. Neutral line tilts are of special interest because of their plausible relationship with MC orientation (Bothmer and Schwenn, 1998; Yurchyshyn et al., 2001; Bothmer, 2003). The tilt γ is defined as the angle measured from the north-south line, following the convention used by Trottet and MacQueen (1980), i.e. a tilt of 0° relates to a vertical neutral line and a tilt of 90° to a horizontal one. Positive tilts correspond to the natural inclination as expected from Joy's law (Hale et al., 1919, see inset in Fig. 1), while negative tilts oppose to those. The absolute values of the tilts have been published in C&B. In addition, the source regions have been classified into those related to active regions (which might have involved a prominence eruption or not, black diamonds) and those related to filaments outside active regions (white squares). Fig. 1 demonstrates no solar cycle variation, though some interesting facts are evident: only very few source regions show negative tilts, mostly in the case of active regions, and tilts greater than 60° are typically found for filaments located in decaying portions of bipolar regions.

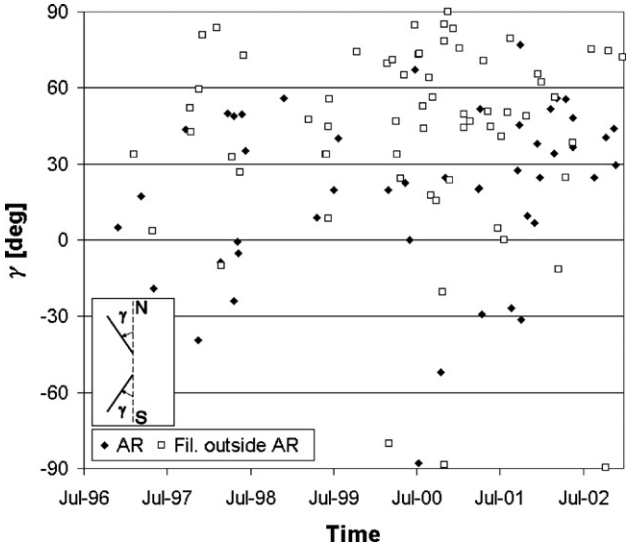

Fig. 1. Tilt angle γ of the structured CMEs' source regions in time. The positive direction of increasing γ is indicated in the inset. Black diamonds represent active regions, while white squares stand for filaments in decaying bipolar regions.

2.2. Latitudinal evolution of the source regions in time

For the analysis of the latitudinal variation, the midpoint of each linear source region was taken as the representative value. The evolution of their latitudes in time is plotted in Fig. 2, together with the longitudinally averaged photospheric magnetic field for the corresponding period of time (provided by courtesy of D. Hathaway). Dark shaded areas refer to negative polarities and bright ones to positive polarities. Once more black diamonds represent active regions while white squares symbolize filaments in decaying portions of bipolar regions. Combining these data with the magnetic field chart reveals that the active region sources (42% of the cases) follow the butterfly diagram. Also apparent from figure is the migration towards higher latitudes of the CMEs' source regions associated with disappearing filaments outside active regions.

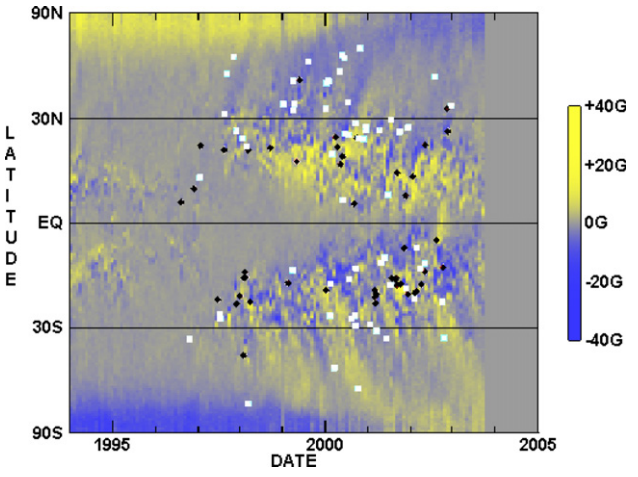

Fig. 2. Latitudinal evolution in time of the structured CMEs' source regions and longitudinally averaged magnetic field, courtesy of NASA/NSST/Hathaway. Black diamonds represent active regions while white squares stand for source regions associated with filaments in decaying bipolar regions. Dark and bright shaded areas represent negative and positive polarities, respectively.

3. CME characteristics

3.1. Evolution of the structured CMEs' position angle

The position angle (PA) is an angular attribute of a feature projected in the plane of the sky, measured counter clockwise from the solar north. The variation of the central position angles derived for the structured CMEs are plotted against time in Fig. 3. The CMEs' central PAs have been sorted in two categories: eastern PAs (0–180°, lower curve) and western PAs (180–360°, upper curve). During low solar activity (year 1996 until mid 1998), there is a clear confinement of PAs to equatorial regions (PA = 90° and PA = 270°), while during solar maximum (years 2000–2002) the PAs fluctuate, reaching even polar PAs (PA = 0° and PA = 180°). These behaviours have also been noticed in other CME datasets, such as those collected by the Solwind (Howard et al., 1985, 1986), SMM (Hundhausen, 1993), MK3 (Cyr et al., 1999) and LASCO (Yashiro et al., 2004) coronagraphs. CMEs apparently positioned above the poles have not necessarily originated from polar latitudes on the sun itself, but it could merely be a matter of projection effects (see C&B). The CME observed on February 27, 2000 (see Fig. 4) is an example for a CME apparently located over the north pole, but which actually originated from a source region located at a latitude of approximately 30°N.

3.2. Evolution of the structured CMEs' deviation

When comparing the PAs of the structured CMEs with those of their associated source regions, it was found that CMEs often do not travel radially outwards with respect to the position of their source regions (e.g., Schwenn, 2000). The deviation of the CME PA with respect to their SR PA was measured as the angular distance between the CME central PA and the PA of the source region's midpoint. The evolution of this quantity in time has been first presented in C&B. A further analysis of the origin of the deviation is investigated here. The evolution of the deviation in time (C&B, Fig. 19) revealed that during times of low solar activity CMEs had been systematically deviated towards the equator with respect to their source regions, while at times of high activity the deviations fluctuated strongly towards the poles or the equator, with no systematic trend.

A good correspondence was found between the deviation of CMEs and the total area of coronal holes (CHs) observed during the corresponding carrington rotation (derived from NSO/KP He 10830 Å data), at times of low solar activity. This suggests that the presence of polar and neighboring CHs affects the outward evolution of CMEs near the Sun. In order to test our assumption on the effects of the CHs on the CME direction of propagation, we introduced the relation given in (1), based on the arbitrary force vector **F**. The process of interaction between CHs and CME expansion and direction of propagation needs to be investigated in more detail to understand more precisely the underlying physics. Certainly, kinetic and magnetic pressures as well as magnetic interactions should be considered, which is beyond the scope of this study. The relationship introduced in (1) by means of the arbitrary force vector **F** is tested empirically. The quantity **F** is representative for the CHs' influence on the CME propagation direction, and accounts for the total deviation force exerted by the CHs on each CME source region. The vector **F** is considered to be directly proportional to the CH area,

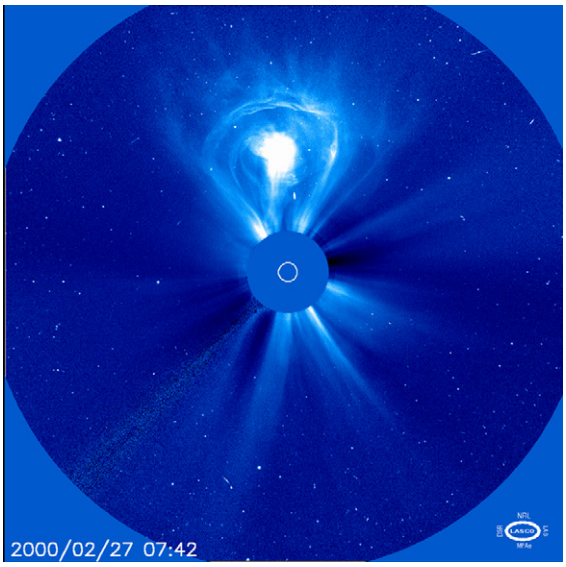

Fig. 4. The CME on February 27, 2000, as observed by the LASCO/C3 coronagraph.

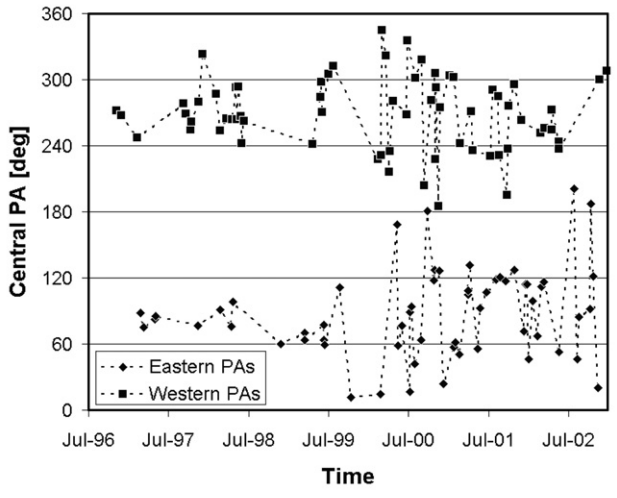

Fig. 3. PA evolution of the structured CMEs. Diamonds represent eastern PAs (0–180°) while squares represent western ones (180–360°).

and inversely proportional to the distance from the CH to the source region's midpoint. The total **F** exerted by the neighboring and polar CHs on an erupting CME is calculated as the sum of the individual contributions from each CH:

$$\mathbf{F} = \sum_i \frac{A_{\mathrm{CH}i}}{|\mathbf{r}_{\mathrm{CH}i}|}\mathbf{u}_{r_{\mathrm{CH}i}}, \quad (1)$$

where $A_{\mathrm{CH}i}$ stands for the area of the ith CH and $|\mathbf{r}_{\mathrm{CHi}}|$ for the distance to the ith CH in the corresponding carrington rotation (see example in Fig. 5). The unity vector $\mathbf{u}_{r_{\mathrm{CH}i}}$ represents the direction of the radius vector $\mathbf{r}_{\mathrm{CH}i}$. Since most of the structured CMEs originated from limb regions, only the elevation component of the net exerted force was taken into account. To analyze deviations in azimuthal direction, a polar view onto the ecliptic is needed, which will be achieved by future missions such as ESA Solar Orbiter or NASA Solar Probe.

The elevation component of the net force **F** (F_{elev}) is compared with the deviation δ of the structured CMEs in Fig. 6. A positive sign in δ and in F_{elev} represents an equatorward direction, while a negative sign stands for poleward directions. Additionally, the data points have been sorted into three time periods according to their behavior evident in Fig. 3. Out of the 62 events with positive δ, i.e. deviation towards the equator, 41 (66%) coincided with a positive F_{elev}. On the other hand, out of the 48 events that exhibited negative deviations, i.e. towards the poles, 37 (77%) matched with negative F_{elev}. Fig. 6 confirms the assumption that neighboring and polar CHs play a major role in the deviation of CMEs. However, other factors are certainly involved as well. External sources of deflections, such as the presence of active regions may play a substantial role, especially at times of minimum solar activity. Intrinsic parameters of CMEs such as its magnetic field configuration and speed (Wang et al., 2004) should also be taken into account for the calculus of the CME deviation. In addition, projection effects may also bias the derived values for the CME deflection.

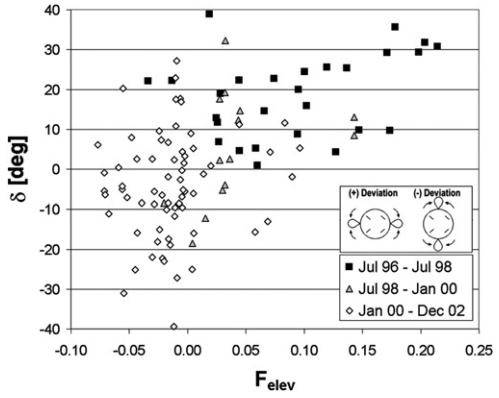

Fig. 6. Dependence of deviation delta on the elevation component of **F**. The force **F** is directly proportional to the CHs' areas and inversely proportional to their distances to the source region. The upper inset indicates that equatorward CME deviations correspond to positive values of δ, while poleward deviations correspond to negative ones. The lower inset denotes the symbols used for the three different periods of time in which the data have been sorted according to their behavior.

4. Summary and conclusions

The analysis presented here was based on a dataset that consists of 124 structured CMEs with identified source regions, mainly located at the solar limb. The events were selected from the full LASCO dataset

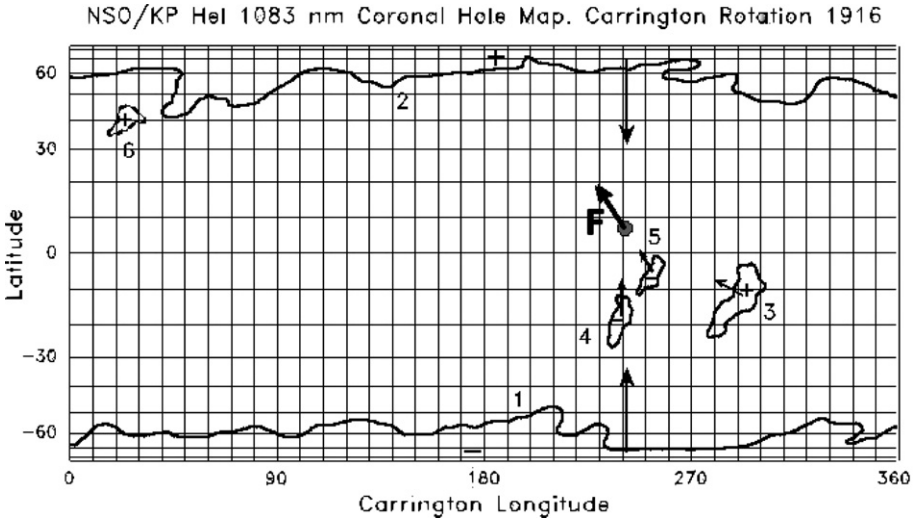

Fig. 5. Synoptic chart for carrington rotation 1916 provided by NSO/KP 10830 Å data. The forces exerted on the source region by the polar and nearby CHs are sketched with arrows. The bold arrow on the source region (here simplified by the midpoint) denotes the magnitude and direction of the net force **F**.

between the years 1996 and 2002 and are listed in Cremades and Bothmer (2004). The properties of this dataset are studied, during the rising and maximum phases of solar cycle 23. The source regions of the structured CMEs were considered as lineal entities given the nature of neutral lines as central features separating regions of opposite polarities. The study of their tilts yielded no systematic variation along the solar cycle. For the latitudinal analysis, the source regions were approximated by their midpoints. Active regions as sources of the structured CMEs showed agreement with the butterfly diagram. On the other hand, source regions of the structured CMEs characterized by disappearing filaments outside active regions relate to the migration of magnetic flux towards polar latitudes.

The confinement of the central PAs of the structured CMEs to equatorial latitudes was obvious during times of solar minimum, while during solar maximum they fluctuated reaching even polar values. The deviation of CMEs with respect to their source regions was always equatorward during the period 1996–1998. In contrast, at times of higher solar activity deviations to high latitudes were also frequent. A further analysis of the deviation yielded a significant correlation with the number of CHs, their area and their distance to the CMEs' source regions. However, this is an empirical test that requires further investigation.

Acknowledgments

This work is part of the scientific investigations of the project Stereo/Corona, in context of the International Max Planck Research School, supported by the German "Bundesministerium für Bildung und Forschung" through the "Deutsche Zentrum für Luft- und Raumfahrt e.V." (DLR, German Space Agency) under Project No. 50 OC 0005. Stereo/Corona is a science and hardware contribution to the optical imaging package SECCHI currently being developed for the NASA STEREO mission to be launched in 2006. Further information can be found at http://stp.gsfc.nasa.gov/missions/stereo/stereo.htm. We thank all the members of the LASCO, EIT and MDI consortiums who built the instruments and provided the data used in this study. LASCO images are courtesy of SOHO/LASCO consortium. SOHO is a project of international cooperation between ESA and NASA. NSO/Kitt Peak data used here are produced cooperatively by NSF/NOAO, NASA/GSFC and NOAA/SEL.

References

Bothmer, V., Schwenn, R. The structure and origin of magnetic clouds in the solar wind. Ann. Geophys. 16, 1–24, 1998.

Bothmer, V. Sources of magnetic helicity over the solar cycle. In: ESA SP-535: Solar Variability as an Input to the Earth's Environment, pp. 419–428, 2003.

Cremades, H., Bothmer, V. On the three-dimensional configuration of coronal mass ejections. A & A 422, 307–322, 2004.

Gosling, J.T., Hildner, E., MacQueen, R.M., et al. Mass ejections from the sun – A view from SKYLAB. J. Geophys. Res. 79, 4581–4587, 1974.

Hale, G.E., Ellerman, F., Nicholson, S.B., Joy, A.H. The Magnetic Polarity of Sun-Spots. ApJ 49, 153–178, 1919.

Howard, R.A., Sheeley Jr., N.R., Koomen, M.J., Michels, D.J. Coronal mass ejections – 1979–1981. J. Geophys. Res. 90, 8173–8191, 1985.

Howard, R.A., Sheeley Jr., N.R., Koomen, M.J., Michels, D.J. The Solar Cycle Dependence of coronal Mass Ejections. In: Marsden, R.G. (Ed.), The Sun and the Heliosphere in Three Dimensions, ASSL, vol. 123. D. Reidel, Norwell, Mass., pp. 107–111, 1986.

Hundhausen, A.J., Sawyer, C.B., House, L., Illing, R.M.E., Wagner, W.J. Coronal mass ejections observed during the solar maximum mission – Latitude distribution and rate of occurrence. J. Geophys. Res. 89, 2639–2646, 1984.

Hundhausen, A.J. Sizes and locations of coronal mass ejections – SMM observations from 1980 and 1984–1989. J. Geophys. Res. 98, 13177–13200, 1993.

Munro, R.H., Gosling, J.T., Hildner, E., et al. The association of coronal mass ejection transients with other forms of solar activity. Solar Phys. 61, 201–215, 1979.

Schwenn, R. Heliospheric 3d Structure and CME Propagation as Seen from SOHO: Recent Lessons for Space weather Predictions. Adv. Space Res. 26, 43–53, 2000.

St. Cyr, O.C., Burkepile, J.T., Hundhausen, A.J., Lecinski, A.R. A comparison of ground-based and spacecraft observations of coronal mass ejections from 1980–1989. J. Geophys. Res. 104, 12493–12506, 1999.

Tousey, R., Howard, R.A., Koomen, M.J. The Frequency and Nature of Coronal Transient Events Observed by OSO-7. BAAS 6, 295, 1974.

Trottet, G., MacQueen, R.M. The orientation of pre-transient coronal magnetic fields. Solar Phys. 68, 177–186, 1980.

Wang, Y., Chenglong, S., Wang, S., Ye, P. Deflection of coronal mass ejection in the interplanetary medium. Solar Phys. 222, 329–343, 2004.

Yashiro, S., Gopalswamy, N., Michalek, G., et al. A catalog of white light coronal mass ejections observed by the SOHO spacecraft. ApJ A18, 7105–7115, 2004.

Yurchyshyn, V.B., Wang, H., Goode, P.R., Deng, Y. Orientation of the Magnetic Fields in Interplanetary Flux Ropes and Solar Filaments. ApJ 563, 381–388, 2001.